Suppression of Poly(ethylene oxide) Crystallization in Diblock Copolymers of Poly(ethylene oxide)-b-poly(ε-caprolactone) Confined to Nanoporous Alumina

ARTICLE *in* MACROMOLECULES · FEBRUARY 2014

Impact Factor: 5.8 · DOI: 10.1021/ma4026477

5 AUTHORS, INCLUDING:

Hatice Duran
TOBB University of Economics and Technology
40 PUBLICATIONS **512** CITATIONS
SEE PROFILE

Martin Steinhart
Universität Osnabrück
181 PUBLICATIONS **5,421** CITATIONS
SEE PROFILE

George Floudas
University of Ioannina
229 PUBLICATIONS **4,182** CITATIONS
SEE PROFILE

Macromolecules

Article

pubs.acs.org/Macromolecules

Suppression of Poly(ethylene oxide) Crystallization in Diblock Copolymers of Poly(ethylene oxide)-*b*-poly(ε-caprolactone) Confined to Nanoporous Alumina

Yasuhito Suzuki,[†] Hatice Duran,[‡] Martin Steinhart,[§] Hans-Jürgen Butt,[†] and George Floudas*[,⊥]

[†]Max-Planck Institute for Polymer Research, 55128 Mainz, Germany

[‡]Department of Materials Science & Nanotechnology Engineering, TOBB University of Economics and Technology, 06560 Ankara, Turkey

[§]Institut für Chemie neuer Materialien, Universität Osnabrück, D-49069 Osnabrück, Germany

[⊥]Department of Physics, University of Ioannina, 45110 Ioannina, Greece

Supporting Information

ABSTRACT: The kinetics of crystallization (heterogeneous vs homogeneous nucleation) and the relation to the local segmental dynamics are studied in a series of poly(ethylene oxide)-*b*-poly(ε-caprolactone) (PEO-*b*-PCL) diblock copolymers confined within self-ordered nanoporous alumina (AAO) by X-ray scattering, polarizing optical microscopy, differential scanning calorimetry and dielectric spectroscopy. In the bulk and for the more asymmetric copolymer, the minority phase (PEO) nucleates solely via homogeneous nucleation. When the same diblock copolymers reside inside AAO, nucleation of PEO is completely suppressed. The majority block (PCL) is also affected by confinement and crystallizes at lower temperatures via homogeneous nucleation. These findings can be discussed in terms of the proposed temperature vs curvature "phase diagram". In this diagram the melt and glassy states are separated by the two nucleation regimes, heterogeneous and homogeneous at high and low temperatures, respectively. Homogeneous nucleation is controlled by the faster part of the distribution of PCL segmental relaxation which under confinement speeds-up.

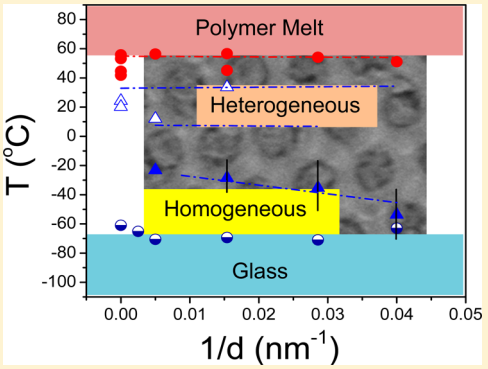

I. INTRODUCTION

In recent years, there have been efforts by different groups in both theory and experiment to understand *how*, *why* and *when* polymers crystallize under confinement.[1−17] This is not only a fundamental problem in polymer physics but has also important technological applications in materials science. For example, the fabrication of polymeric materials with predetermined crystallinity can result in materials with controlled mechanical and optical properties. Of central importance to this discussion is the origin of heterogeneous and homogeneous nucleation and their possible relation to the freezing of the local segmental dynamics at the liquid-to-glass temperature. Most homopolymers crystallize at low undercoolings via heterogeneous nucleation. *Heterogeneous* nucleation is initiated by external means such as additives, interfaces and possibly interphases. Heterogeneous nuclei are already present at the beginning of nucleation, hence heterogeneous nucleation is athermal and either secondary or tertiary. *Homogeneous* nucleation involves the spontaneous clustering of several segments and the formation and growth of larger stable nuclei above a critical size. Homogeneous nucleation is primary and thermal. Because homogeneous nucleation takes place at large undercoolings, it is inevitably coupled with the *spatio-temporal* heterogeneities associated with the liquid-to-glass temperature.[18,19]

Self-ordered nanoporous aluminum oxide (AAO)[20−22] contains arrays of parallel, cylindrical nanopores that can be employed as model system[4−6,13−16,23,24] in studying the effect of confinement on polymer crystallization. Recent studies of polymer crystallization in AAO revealed different nucleation mechanisms. For example, poly(ethylene oxide) (PEO) crystallizes homogeneously in narrow pores.[5] However, poly(ε-caprolactone) (PCL) crystallizes via several heterogeneous nucleation events at lower undercoolings and via homogeneous nucleation within the smaller pores.[6]

Diblock copolymers comprising crystallizable blocks provide additional parameter space for studying the effect of confinement.[8,25−28] Polymer crystallization in bulk diblock copolymers is classified as confined, template and breakout, depending on the value of the product χN (where χ is the interaction parameter and N the total degree of polymerization) at the crystallization temperature with respect to the value at the order-to-disorder transition temperature.[8] Placing block co-

Received: December 27, 2013
Revised: February 7, 2014
Published: February 27, 2014

   dx.doi.org/10.1021/ma4026477 | *Macromolecules* 2014, 47, 1793−1800

Table 1. Molecular Characteristics and Degrees of Crystallinity of the PEO-*b*-PCL Block Copolymers

sample	$M_{n,PEO}$ (g/mol)	$M_{n,PCL}$ (g/mol)	PDI_{PCL}	f_{PEO} [a]	X_c^{PEO} [b] (%)	X_c^{PCL} [c] (%)
PEO_{114}-*b*-PCL_{88}	5000	10 000	1.19	0.32	41	37
PEO_{114}-*b*-PCL_{158}	5000	18 000	1.48	0.21	37	47
PEO_{114}-*b*-PCL_{325}	5000	37 000	1.80	0.11	25	27

[a] f_{PEO} is the PEO volume fraction based on PEO and PCL densities of 1.239 and 1.187 g/cm^3, respectively. [b] From DSC based on ΔH_0 = 200 J/g. [c] From DSC based on ΔH_0 = 148 J/g.

polymers under the extrinsic hard confinement provided by AAO introduces additional parameters such a surface−polymer interactions and structural frustration related to incommensurability of the domain spacing to the pore diameter. Here we investigate the confined crystallization of double crystalline diblock copolymers of PEO-*b*-PCL within AAO. The crystallization in bulk PEO-*b*-PCL was already reported.[29−31] When PEO-*b*-PCL is located inside AAO, the PEO chains are subjected to double confinement: (1) confinement imposed by PCL crystals, which grow in bulk PEO-*b*-PCL at higher crystallization temperatures than PEO crystals and (2) hard confinement imposed by the rigid AAO pore walls. The investigation is made as a function of copolymer composition, pore size and heating/cooling rate with structural (X-ray scattering, polarizing optical microscopy), thermodynamic (DSC), and dynamic (dielectric spectroscopy) means. Although both homopolymers could crystallize homogeneously at large undercoolings, one of the blocks (PEO) in PEO-*b*-PCL confined to AAO is unable to crystallize under conditions where PCL crystallizes. Hence, the double soft/hart confinement imposed by the block copolymer domain structure and AAO pore geometry facilitates further control over crystallinity and thus on the final mechanical properties of copolymer nanostructures with crystallizable blocks. We propose that confinement effects can be discussed in terms of the pertinent temperature vs. curvature "phase diagram".[32,33] There, the equilibrium melt and nonergodic glassy states at higher and lower temperatures, respectively, are separated by the two nucleation regimes (heterogeneous and homogeneous). We explore the effect of proximity of nucleation regimes to these boundary states.

II. EXPERIMENTAL SECTION

Samples and Methods of Infiltration. Poly(ethylene oxide-*b*-ε-caprolactone) (PEO-*b*-PCL) samples with three different molecular weights (Table 1) were obtained from Polymer Source Inc. and used as received. Self-ordered AAO (pore diameters of 25, 35, 65, 200, and 400 nm; pore depth 100 μm) was prepared following the procedures reported in the literature.[20−22] Infiltration of the PEO-*b*-PCL was performed by placing neat PEO-*b*-PCL on the surface of the self-ordered AAO at 100 °C for 12 h under vacuum. At this temperature all block copolymers studied here flow as they are in the disordered state (see below). Prior to the DSC and dielectric spectroscopy (DS) experiments, excess amount of PEO-*b*-PCL was removed from the surface of the self-ordered AAO membranes with razor blades and soft polishing paper (Buehler Microcloth).

Polarizing Optical Microscopy. The real-time crystallization and melting of the bulk PEO-*b*-PCL samples was monitored by polarizing optical microscopy (POM). A thin PEO-*b*-PCL film (thickness of 50 μm maintained by Teflon spacers) was placed between two glass plates and introduced into a Linkam THMS 600 hot plate under an Axioskope 40 FL optical microscope equipped with a video camera and a fast frame grabber. Starting from the melt state (85 °C), the samples were quickly cooled (50 °C/min) to different final crystallization temperatures and the isothermal crystallization was observed within the temperature range 40−58 °C in the three copolymers. With the aid of a software, the evolution of spherulitic radii was determined for different time-intervals. Subsequently, the (linear) growth rates G were obtained.

X-ray Scattering. Wide-angle X-ray scattering in the $\theta/2\theta$ geometry was carried out with a D8 Advance X-ray diffractometer (Bruker) operated at a voltage of 40 kV and a current of 30 mA. An aperture (divergence) slit of 0.3 mm, a scattered-radiation (antiscatter) slit of 0.3 mm together with a monochromator slit of 0.1 mm and a detector slit of 1 mm were employed. Measurements were performed with Cu K_α radiation (a graphite monochromator was located between detector slit and detector) detected by a scintillation counter with 95% quantum yield for Cu Kα radiation. Scans in the 2θ-range from 5 to 40° in steps of 0.01° were performed at selected temperatures. Prior to any measurement, PEO-*b*-PCL was heated to 85 °C and slowly cooled down to room temperature (~3 °C/min). Following this, measurements were made on heating in 5 °C temperature intervals, after equilibrating at each temperature for 1 h, up to complete melting of both blocks. Additional measurements were made at lower temperatures (−40 and −60 °C). Small-angle X-ray scattering (SAXS) measurements were carried out on bulk PEO-*b*-PCL as well as on PEO and PCL homopolymers (PCL M_w = 8900 g/mol and PEO M_w = 2000, 5000, and 8000 g/mol) at selected temperatures in the range from 30 to 60 °C. SAXS measurements were carried out with a Rigaku RA-Micro 7 desktop rotating anode X-ray generator with a maximum power of 800 W and brightness of 18 kW/mm^2 (operated at a tube voltage of 40 kV and tube current of I = 10 mA (400 W)) utilizing a Cu target. The detection system was a MAR345 image plate area detector and the sample-to-detector distance was set at 2.24 m. Measurements from extruded fibers (extrusion temperature 25 °C) were done within the temperature range from 30 to 80 °C in 5 °C intervals following equilibration for 1h and subsequent measuring time of 1h at each selected temperature on heating. From the recorded 2-D diffraction patterns the intensity distributions were obtained and are presented as a function of the scattering vector q ($q = (4\pi/\lambda)\sin(2\theta/2)$, where 2θ is the scattering angle).

Differential Scanning Calorimetry (DSC). Thermal analysis was carried out using a Mettler Toledo differential scanning calorimeter (DSC-822). DSC traces of neat PEO-*b*-PCL copolymers were acquired using an empty pan as reference. The PEO-*b*-PCL mass in PEO-*b*-PCL-infiltrated AAO was estimated from the mass difference between PEO-*b*-PCL infiltrated self-ordered AAO and empty self-ordered AAO. Samples were weighed with a Mettler Toledo AX205 balance. Prior to any DSC measurement, the Al substrates to which the AAO layers had been connected were etched with solutions containing 1.7 mg $CuCl_2{\cdot}2H_2O$, 50 mL deionized H_2O and 50 mL concentrated HCl(aq) under cooling with ice water. Subsequently, the samples were further milled to pellets, and 0.9−5.5 mg sample material was sealed in aluminum pans (100 μL). DSC traces of PEO-*b*-PCL-infiltrated self-ordered AAO were recorded using reference pans containing empty AAO pieces of the same pore diameter. All samples were first cooled at a rate of 10 K/min from ambient temperature to 173 K and then heated to 393 K at the same rate under a nitrogen atmosphere. The same cycle was repeated two times. Melting and crystallization points, as well as heats of fusion and of crystallization, were determined from the second heating and cooling thermographs, respectively.

Dielectric Spectroscopy. Dielectric spectroscopy (DS) measurements were performed at different temperatures in the range of 183−348 K, at atmospheric pressure, and for frequencies in the range from 10^{-2} to 10^7 Hz using a Novocontrol Alpha frequency analyzer

dx.doi.org/10.1021/ma4026477 | Macromolecules 2014, 47, 1793−1800

composed of a broadband dielectric converter and an active sample hand. For bulk PEO-*b*-PCLs, the DS measurements were carried out in the usual parallel plate geometry with electrodes of 20 mm in diameter and a sample thickness of 50 μm maintained by Teflon spacers. For the PEO-*b*-PCL infiltrated self-ordered AAO samples, a 10 mm electrode was placed on the AAO surface. In all cases, the complex dielectric permittivity $\varepsilon^* = \varepsilon' - i\varepsilon''$, where ε' is the real and ε'' is the imaginary part, was obtained as a function of frequency ω and temperature T, *i.e.*, $\varepsilon^*(T, \omega)$.[34−36] The measured dielectric spectra were corrected for the geometry by using two capacitors in parallel (composed of $\varepsilon^*_{PEO-PCL}$ and ε^*_{AAO} and the measured total impedance was related to the individual values through $1/Z^* = 1/Z^*_{PEO-PCL} + 1/Z^*_{AAO}$).[37] This allows calculating the real and imaginary parts of the dielectric permittivity as a function of the respective volume fractions. The latter were estimated by digitization of the scanning electron microscopy (SEM) images of empty AAO templates (SEM images were obtained using a LEO Gemini 1530 SEM, operated at acceleration voltages from 0.75 to 6 kV with in-lense secondary electron detectors, that are most suitable for this type of analysis). The analysis was done using the empirical equation of Havriliak and Negami:[38]

$$\varepsilon^*_{HN}(\omega, T) = \varepsilon_\infty(T) + \frac{\Delta\varepsilon(T)}{[1 + (i\omega\cdot\tau_{HN}(T))^m]^n} + \frac{\sigma_0(T)}{i\varepsilon_f\omega} \quad (1)$$

Here, $\Delta\varepsilon(T)$ is the relaxation strength of the process under investigation, τ_{HN} is the relaxation time of the equation and m, n ($m > 0$, $mn \leq 1$) describe the symmetrical and asymmetrical broadening of the distribution of relaxation times and ε_∞ is the dielectric permittivity at the limit of high frequencies. The relaxation times at maximum loss (τ_{max}) are presented herein and have been analytically obtained by the Havriliak−Negami equation as follows:

$$\tau_{max} = \tau_{HN} \sin^{-1/m}\left(\frac{\pi m}{2(1+n)}\right) \sin^{1/m}\left(\frac{\pi mn}{2(1+n)}\right) \quad (2)$$

At lower frequencies, ε'' rises due to the conductivity ($\varepsilon'' = \sigma/(\omega\varepsilon_f)$, where σ is the dc conductivity and ε_f the permittivity of free space). The conductivity contribution has also been taken into account during the fitting process. The measured ε'' spectra have been used for the analysis except at high temperatures where the derivative of ε' has been employed ($d\varepsilon'/d[\ln \omega] \sim -(2/\pi)\varepsilon''$). This method is useful in fitting relaxation processes which are hidden under the conductivity, provided that the system is free of surface polarization effects.

III. RESULTS AND DISCUSSION

a. Self-Assembly and Dynamics in Bulk. The crystalline structure in the three diblock copolymers is discussed at the different pertinent length scales. The unit cell, nanodomain morphology, and spherulitic superstructure are obtained from wide-angle X-ray scattering (WAXS), small-angle X-ray scattering (SAXS) and polarizing optical microscopy (POM), respectively. WAXS on PEO-*b*-PCL revealed mixed scattering patterns with reflections that can be assigned to monoclinic PEO[39] and orthorhombic PCL.[40] As an example, the WAXS patterns of PEO_{114}-*b*-PCL_{88} displayed in Figure 1 show the (120) and (032) reflections of monoclinic PEO at $2\theta = 19.5°$ and $2\theta = 23.2°$. The monoclinic PEO unit cell contains four PEO chains, each of which forms a 7/2 helix.[39] On the other hand, the (110), (111) and (200) reflections of orthorhombic PCL appear at 2θ angles of 21.3°, 21.9° and 23.6°. The PCL unit cell is composed from two chains with opposite orientation in an extended planar conformation.[40]

The appearance of PEO and PCL reflections in the WAXS patterns indicates the existence of regions in which PEO crystals are enriched and a high portion of PCL chains is incorporated in amorphous interphases as well as of different regions where now PCL crystals dominate and PEO chains are

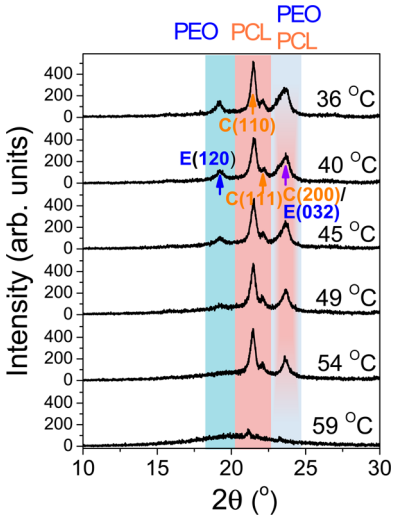

Figure 1. WAXS patterns measured in $\theta/2\theta$ geometry of bulk PEO_{114}-*b*-PCL_{88} at different temperatures. Letters E and C denote reflections of monoclinic PEO and orthorhombic PCL. The corresponding Miller indices are indicated. Blue and red areas indicate 2θ ranges in which PEO and PCL reflections appear. The (200) reflection of PCL and the (032) reflection PEO coincide at $2\theta = 23.6°$.

incorporated in amorphous interphases. Local suppression of crystallization of one block in the same double crystalline block copolymers was first reported in ref 29. Basically, it is a consequence of the fact that both blocks would have to crystallize in different unit cells. On heating PEO_{114}-*b*-PCL_{88} (Figure 1), the PEO crystals melt at first at about 55 °C, whereas PCL crystals melt at about 65 °C. The WAXS patterns of the three PEO-*b*-PCLs are compared in Figure S1 (Supporting Information), revealing reduced PEO crystallinity in the more asymmetric block copolymers.

Information on the state of the block copolymers prior to crystallization and on the nanodomain morphology following crystallization can be obtained from SAXS. Figure 2 shows the SAXS patterns of an oriented PEO_{114}-*b*-PCL_{88} fiber as a

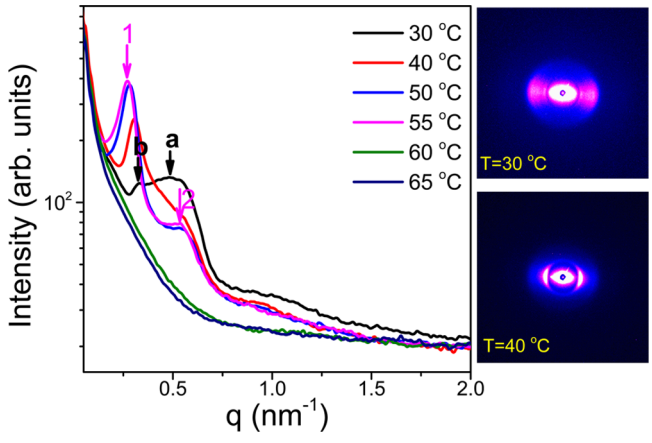

Figure 2. (Left) SAXS patterns of bulk PEO_{114}-*b*-PCL_{88} at different temperatures as indicated At 30 °C, a and b indicate the approximate peak positions associated with PEO and PCL crystals, respectively. The positions of the scattering vectors corresponding to the first and higher order reflections are shown for 55 °C. (Right) 2D-SAXS images obtained from extruded PEO_{114}-*b*-PCL_{88} fibers at 30 (top) and 40 °C (bottom).

dx.doi.org/10.1021/ma4026477 | *Macromolecules* 2014, 47, 1793−1800

function of temperature. At temperatures above the melting point of both blocks (i.e., $T > 65$ °C) the scattering pattern does not contain any sharp peaks except a broad feature at lower scattering vectors, indicating that the block copolymer is disordered. Hence, the crystallization of PCL and PEO from the disordered melt drives the phase separation at lower temperatures in agreement with earlier reports.[31] The SAXS pattern at 30 °C is composed from a very broad peak around $q \sim 0.5$ nm^{-1} superimposed on a sharper peak at $q \sim 0.32$ nm^{-1}. The broad feature (denoted *a* in Figure 2) is associated with PEO crystals having average correlation distances in the range 13−19 nm. The narrower feature (denoted *b* in Figure 2) reflects correlations of PCL crystals with an average distance of ∼19.6 nm. On heating, at about 50 °C, PEO crystals melt leaving only PCL crystals with an average correlation distance of 23.5 nm. These results are supported by the DSC traces (below).

Figure 3 shows the DSC traces of the three block copolymers on cooling and subsequent heating at a rate of 10 K/min. On

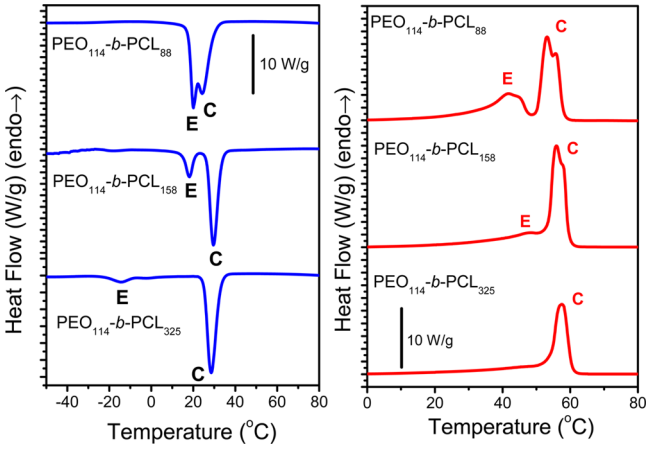

Figure 3. Cooling (left) and subsequent heating (right) thermograms of bulk PEO-*b*-PCL (heating/cooling rate 10 K/min). Letters **E** and **C** denote crystallization/melting peaks of PEO and PCL, respectively.

cooling PEO_{114}-*b*-PCL_{88}, PCL crystallizes first (at ∼25 °C) followed by the crystallization of PEO (at ∼20 °C). On subsequent heating, PEO exhibits a broad melting peak ranging from 25 to 48 °C, in agreement with WAXS indicating a broad distribution of PEO crystal sizes (Figure 1). PCL crystals melt at higher temperatures with a dual melting peak reflecting melting of crystals of two different sizes. In PEO_{114}-*b*-PCL_{158}, PCL crystallizes at 29.6 °C followed by PEO crystallization at ∼18.1 °C. On subsequent heating, there is again a broad PEO melting peak centered around 48 °C, followed by melting of PCL crystals. In general, the more asymmetric the investigated PEO-*b*-PCL is, the lower is the PEO crystallization temperature. This is more evident in PEO_{114}-*b*-PCL_{325}. Here, PCL crystallizes at 28.5 °C whereas PEO crystallization is shifted to −14.6 °C. The decrease in the PEO crystallization temperature can be understood by the confinement of PEO chains imposed by PCL crystals. A similar effect has recently found when PEO confined to self-ordered AAO was crystallized.[5] Confinement in pores with diameters below 200 nm resulted in homogeneous crystallization of PEO at substantially lower temperatures as in the case of PEO-*b*-PCL confined to AAO. The extracted degrees of crystallinity for both PEO and PCL chains ($X_c = \Delta H/w\Delta H_0$, where ΔH is the measured heat of fusion, ΔH_0 is the heat of fusion of an "ideal" crystal and w is the weight fraction of PEO or PCL in the diblocks) are listed in Table 1.

The complex dielectric permittivity, ε^*, is also a sensitive probe of the structural and dynamic changes in the block copolymers. It has been shown earlier that the temperature dependence of dielectric permittivity and loss can be used as fingerprints of phase transitions.[32,33] Figure 4 shows the

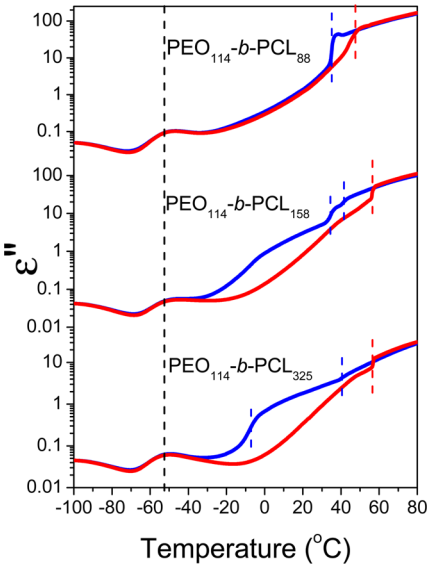

Figure 4. Isochronal dielectric loss curves (blue, cooling; red, heating) of bulk PEO_{114}-*b*-PCL_{88} obtained at a frequency of 1154 Hz (heating/cooling rate 2 K/min). Dashed lines indicate crystallization temperatures (blue), melting temperatures (red) and the location of the segmental process (black), respectively.

dielectric loss curves of the three copolymers on cooling and subsequent heating (with a rate of 2 K/min) under isochronal conditions (f = 1154 Hz). On cooling, PCL and PEO crystallization are better separated as shown by the blue dashed curves. For example, in PEO_{114}-*b*-PCL_{158}, the two crystallization temperatures are different by 10 K in agreement with the DSC result. In PEO_{114}-*b*-PCL_{325}, PCL and PEO crystallization temperatures are separated by about 45 °C which is also in qualitative agreement with the DSC curves despite different cooling rates were applied. New information from the isochronal DS measurements is the dielectric loss peak at about −52 °C that, as we will discuss below (with respect to Figure 5), associates with the molecular dynamics of amorphous PCL segments.

The local segmental dynamics in the block copolymers can be obtained from DS under isothermal conditions. DS in the block copolymers follows the relaxation of the larger dipole moment associated with the PCL repeat unit [−$(CH_2)_5$COO−]. It amounts to 1.72 D with components parallel (∼0.64 D) and perpendicular (∼1.6 D) to the backbone as obtained from dilute solutions in dioxane.[41] Thus, DS is capable, in principle, to follow the local and global PCL chain dynamics by recording dielectric spectra as a function of frequency at different temperatures. Nevertheless, a strong contribution from ionic conductivity and the presence of crystalline/amorphous domains and the associated Maxwell−Wagner−Sillars polarization[34] precludes the investigation of the slower chain dynamics in the bulk state. On the other hand, PEO has a weaker dipole moment (1.04 D)[42] than PCL.

dx.doi.org/10.1021/ma4026477 | *Macromolecules* 2014, 47, 1793−1800

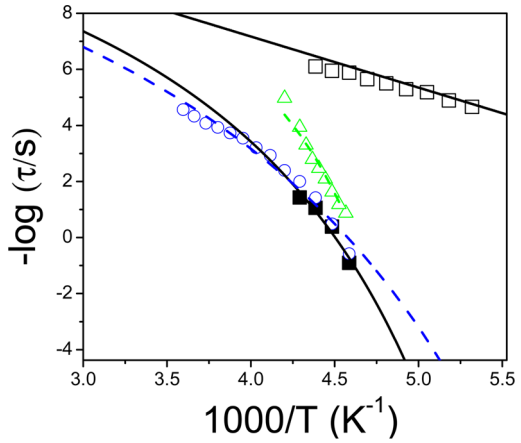

Figure 5. Relaxation times at maximum loss of bulk PEO_{114}-*b*-PCL_{88}. The α- (filled squares) and β- (open squares) processes are shown. Black lines represent fits to the VFT and Arrhenius equations. The α-relaxation times of bulk PEO (open triangles) and bulk PCL (open circles) are shown for comparison.

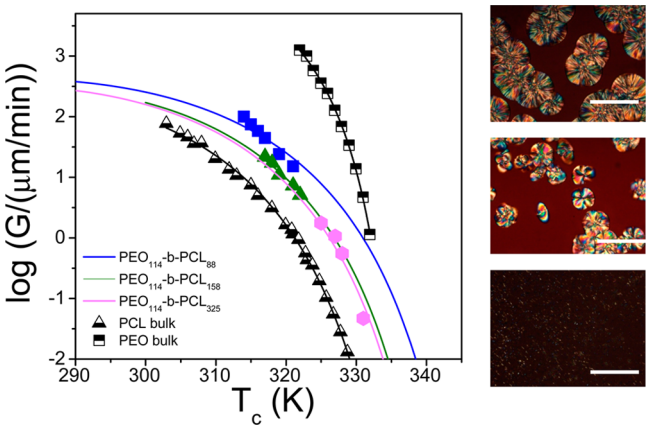

Figure 6. (Left) Spherulitic growth rates plotted as a function of temperature for PEO_{114}-*b*-PCL_{88} (blue squares), PEO_{114}-*b*-PCL_{158} (green triangles), PEO_{114}-*b*-PCL_{325} (magenta hexagons), PEO homopolymer (black squares) and PCL homopolymer (black triangles). The lines are fits according to the Lauritzen-Hoffman and Strobl theories. (Right) POM images of PEO_{114}-*b*-PCL_{88} (top, T = 43 °C), PEO_{114}-*b*-PCL_{158} (middle, T = 46 °C) and PEO_{114}-*b*-PCL_{325} (bottom, T = 54 °C), respectively. The scale bars correspond to 50 μm.

Taking into account the small volume fraction of the minority component PEO, contributions of PEO are not visible in the dielectric spectra. We are thus focusing our attention on PCL local dynamics in the three copolymers.

The α- and β- processes in bulk PEO_{114}-*b*-PCL_{88} were fitted according to the HN function (eq 2) with respective shape parameters m = 0.55 n = 0.50 and m = 0.16, n = 0.22. Typical dielectric loss curves are depicted in Figure S2, Supporting Information, at temperatures corresponding to the segmental (α-) and local (β-) processes. The two processes in PEO_{114}-*b*-PCL_{88} have distinctly different T-dependencies and are shown in Figure 5 together with the bulk PEO and PCL times. The α-process in the copolymers conforms to the Vogel–Fulcher–Tammann (VFT) equation:

$$\tau = \tau_o \exp\left(\frac{B}{T - T_o}\right) \quad (3)$$

where τ_o (=10^{-12} s; held fixed because of the limited frequency range) is the relaxation time in the limit of very high temperatures, B (=1940 K) is the activation parameter and T_0 (=152 K) is the "ideal" glass temperature. The conventional glass temperature is obtained from the above equation when the α-relaxation time amounts to 100 s. The values of these parameters are in proximity to the PCL homopolymer values (also shown in Figure 5). The β-process conforms to an Arrhenius equation, $\tau = \tau_o \exp(E/RT)$, with $\tau_o = 1.4 \times 10^{-13}$ s and an activation energy, E, of 29.4 kJ/mol.

The superstructure formation in the block copolymers was subsequently studied by POM. Measurements were made isothermally following quenching from the isotropic phase to different final crystallization temperatures. Figure 6 displays the growth rates of the superstructures that are associated with PCL crystals. Initially, the PCL crystals consist of elongated (axialitic) objects that are converted into spherulites as crystal growth proceeds. The growth rates of PCL superstructures can be fitted according to the Lauritzen–Hoffman theory[43] or by the recent modification proposed by Strobl.[44] According to the latter model, the growth rate of a superstructure contains two terms with opposite temperature dependence:

$$G = G_0\left(-\frac{B}{T - T_0}\right)\exp\left(-\frac{K_g}{(T_{zg} - T)T}\right) \quad (4)$$

The first term refers to the segmental mobility according to the VFT eq 3 that reflects the dynamics of amorphous PCL segments. The second term reflects the free energy of activation for the placement of a secondary nucleus on the growth face. T_{zg} is the zero-growth temperature, i.e., the temperature above which the superstructures cannot grow.[41] The obtained T_{zg} values were 357, 353, and 353 K, respectively, for PEO_{114}-*b*-PCL_{88}, PEO_{114}-*b*-PCL_{158} and PEO_{114}-*b*-PCL_{325}. In the same Figure the growth rates of PCL and PEO homopolymers are included. Evidently, the growth rates of the formed superstructures in the three copolymers can be attributed to crystals formed by the PCL blocks as indicated by two observations. First, the temperature dependence of the growth rates are more similar to the growth rates of PCL homopolymer crystals than to those of PEO homopolymer crystals (Figure 6). Second, the evolution of the growth shapes in the course of crystal growth (from axialites to spherulites) resembles that observed for PCL homopolymers. PEO, on the other hand, was found to crystallize in the background of the already impinged PCL spherulites in much larger spherulitic domains in the PEO_{114}-*b*-PCL_{88} with the higher PEO content and the higher PEO crystallinity (Table 1). This again confirms the preferential nucleation of PCL or PEO chains in the superstructures.

Thus, in the bulk block copolymers it is crystallization that drives phase separation. In this case, both blocks are able to crystallize via heterogeneous nucleation. However, in the more asymmetric copolymer, the minority block (PEO) is able to crystallize only at lower temperatures by homogeneous nucleation.

b. Block Copolymer Self-Assembly and Dynamics under Hard Confinement. The most dramatic effect of the hard confinement imposed by the rigid AAO pore walls on PEO-*b*-PCL is suppression of PEO crystallization. This is evident, for example, in the WAXS patterns of PEO_{114}-*b*-PCL_{88} obtained at temperatures of −40 and −60 °C shown in Figure

dx.doi.org/10.1021/ma4026477 | *Macromolecules* 2014, 47, 1793–1800

7. The reason for performing WAXS measurements at such low temperatures will become clearer later (see discussion of DSC

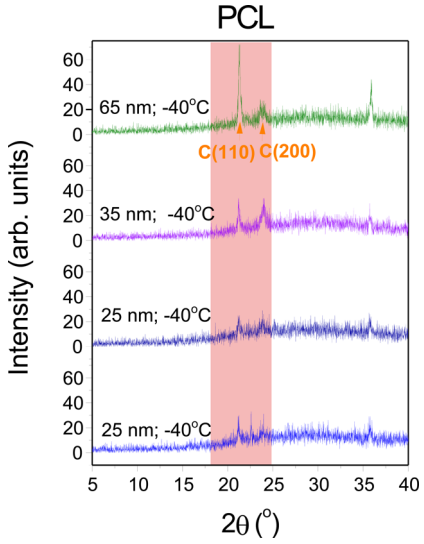

Figure 7. WAXS patterns measured in $\theta/2\theta$ geometry of PEO_{114}-*b*-PCL_{88} located inside self-ordered AAO with pore diameters ranging from 65 to 25 nm at −40 and −60 °C. The main PCL reflections (C) are indicated.

curves of PEO-*b*-PCL confined to AAO below). Here we only mention that at such temperatures both PCL and PEO homopolymers would crystallize either heterogeneously and/or homogeneously. However, the WAXS pattern of PEO_{114}-*b*-PCL_{88} inside self-ordered AAO contains only a subset of the reflections appearing in WAXS patterns of bulk PEO_{114}-*b*-PCL_{88} (Figure 1), namely the (110) and (200) reflections of orthorhombic PCL. The selective appearance of these reflections indicates preferred orientation of the {110} and {200} faces normal to the AAO pore axes. We mention here that the same preferred orientation was found in PCL homopolymer located inside self-ordered AAO.[6] Schulz scans in that case revealed Herrmans orientation parameter of ∼0.95, suggesting a nearly uniform orientation of the {110} crystal faces perpendicular to the AAO pore axes.[6]

The effect of the hard confinement imposed by the rigid AAO pore walls on the type of nucleation process initiating crystallization in PEO-*b*-PCL can be studied by DSC. Figure 8 shows DSC cooling traces and the subsequent heating traces (rate 10 K/min) of PEO_{114}-*b*-PCL_{88} inside self-ordered AAO in comparison to bulk PEO_{114}-*b*-PCL_{88}. As discussed above, DCS cooling runs of bulk PEO_{114}-*b*-PCL_{88} show a dual exothermic peak associated with PCL (peak at 25 °C) and PEO (peak at 20 °C) crystallization. The DSC traces of PEO_{114}-*b*-PCL_{88} confined to AAO reveal completely different crystallization behavior. Now the main crystallization peak is at lower temperatures and upon confinement shifts to even lower temperatures, from ∼ −26 °C in 65 nm pores to about −53 °C in 25 nm pores. A weak exothermic peak is also visible at higher temperatures in some of the traces. These DSC traces can be interpreted with the aid of the WAXS results. Within self-ordered AAO only PCL can crystallize. Thus, the exothermic peaks in the DSC curves reflect solely crystallization of PCL crystals. We attribute the weak exothermic peak at higher temperatures to PCL heterogeneous nucleation as found also in bulk PCL. Heterogeneous crystallization is a minor crystal-

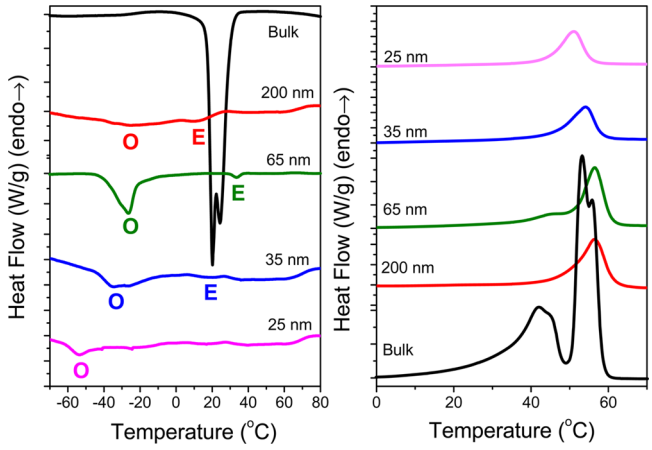

Figure 8. Cooling (left) and subsequent heating (right) thermograms of bulk PEO_{114}-*b*-PCL_{88} and PEO_{114}-*b*-PCL_{88} located inside self-ordered AAO with pore diameters ranging from 400 to 25 nm (heating/cooling rate 10 K/min). DSC thermograms of the corresponding bulk block copolymers are shown for comparison. Letters E and O denote heterogeneous and homogeneous nucleation, respectively.

lization mechanism in the smaller pores. Heterogeneous nucleation in the large pores can be explained as follows. The spherulite diameters (Figure 6) of PCL crystals upon impingement are ∼250, 100, and 40 μm, respectively, in PEO_{114}-*b*-PCL_{88}, PEO_{114}-*b*-PCL_{158}, and PEO_{114}-*b*-PCL_{325}. This allows estimating the volume per heterogeneous nuclei, which is about $\sim10^{-2}$, $\sim10^{-4}$, and $\sim10^{-5}$ mm^3 in PEO_{114}-*b*-PCL_{88}, PEO_{114}-*b*-PCL_{158}, and PEO_{114}-*b*-PCL_{325}. However, within AAO, the copolymers are confined to discrete cylindrical pores with volumes in the range from 3×10^{-9} mm^3 (pore diameter 200 nm, pore depth 100 μm) to 5×10^{-11} mm^3 (pore diameter 25 nm, pore depth 100 μm). Since these pore volumes are several orders of magnitude smaller than the volume per heterogeneous nucleus in bulk PEO-*b*-PCL, only a minor fraction of pores will contain heterogeneous nuclei. The crystallization peak denoted E in the DSC traces of Figure 8 can be ascribed to PCL located in AAO pores containing heterogeneous nuclei.

The probability of heterogeneous nucleation in the smaller pores is negligible; PCL in the smaller pores can only nucleate by crossing the intrinsic barrier for homogeneous nucleation. The critical nucleus size for homogeneous nucleation, l^*, is given by[43] $l^* = 4\sigma_e T_m^\circ/\Delta T \Delta H_m \rho_c$, where σ_e (106 and 93 mJ/m^2 for PCL and PEO, respectively)[45−47] is the fold surface free energy, T_m° (348 and 331 K for PCL and PEO, respectively) the equilibrium melting temperature, ΔH_0 (148 and 200 J/g for PCL and PEO, respectively) the latent heat of fusion at the equilibrium melting temperature,[45−47] $\Delta T = T_m^0 - T_c$ the undercooling and ρ_c (1.187 and 1.239 g/cm^3, respectively, for PCL and PEO) the crystal density. For the PCL block in PEO_{114}-*b*-PCL_{88} ΔT is 30 K, but it increases to 105 K for PEO_{114}-*b*-PCL_{88} inside self-ordered AAO with a pore diameter of 25 nm. At such undercooling, the critical nucleus size for homogeneous PCL nucleation is about 8 nm and, therefore, smaller than the diameter of the smallest pores. Thus, the PCL blocks of PEO-*b*-PCL are able to crystallize even within 25 nm pores. However, the onset of PCL crystallization limits the available space for PEO crystallization. Homogeneous nucleation of PEO at an undercooling of ΔT = 100 K requires a crtitical nucleus size of ∼5 nm and this size increases at higher temperatures, i.e., by

dx.doi.org/10.1021/ma4026477 | Macromolecules 2014, 47, 1793−1800

decreasing ΔT. Thus, PEO chains in PEO-*b*-PCL located within self-ordered AAO remain amorphous, being restricted by the rigid AAO pores walls and by PCL crystals already formed.

In a recent study[6] we proposed a relation of the homogeneous nucleation process with the *spatiotemporal* heterogeneity associated with the liquid-to-glass temperature. To explore ths relationship in the present system, we have carried out DS measurements on PEO_{114}-*b*-PCL_{88} located inside self-ordered AAO in comparison to bulk PEO_{114}-*b*-PCL_{88}. The results for the segmental dynamics are shown in the Arrhenius representation of Figure 9. There is a speed-up of the

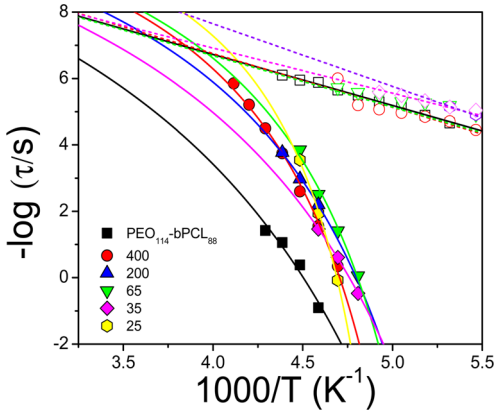

Figure 9. Relaxation times at maximum loss corresponding to the PCL α- and β- processes in bulk PEO_{114}-*b*-PCL_{88} and in PEO_{114}-*b*-PCL_{88} confinement to AAO with pore diameters ranging from 400 to 25 nm; (squares): bulk PEO_{114}-*b*-PCL_{88} and PEO_{114}-*b*-PCL_{88} within self-ordered AAO with a pore diameter of 400 nm (circles), 200 nm (up triangles), 65 nm (down triangles), 35 nm (rhombi) and 25 nm (hexagons). Solid and dashed lines indicate fits to the α- and β-processes, respectively, with the VFT and Arrhenius equations.

PCL segmental dynamics in PEO_{114}-*b*-PCL_{88} inside self-ordered AAO with respect to bulk PEO-*b*-PCL and only a minor effect on the local β-process. In addition, the effect of confinement is to broaden the distribution of relaxation times associated with the segmental process (Figure S3 of the Supporting Information). These affects are not uncommon to the dynamics of confined polymers.[2,17,48]

The modifications of nucleation behavior and local segmental dynamics of PEO_{114}-*b*-PCL_{88} related to the hard confinement imposed by the rigid AAO pores on the copolymers can best be discussed in terms of the "phase-diagram" of Figure 10. This diagram is based on the DSC results obtained on cooling (heterogeneous vs. homogeneous nucleation) and heating (apparent melting temperatures) as well as on the liquid-to-glass temperatures obtained from DS (T_g is operationally defined as the temperature where the segmental time is at $\tau \sim 100$ s). Figure 10 depicts the polymer melt state at high temperatures separated from the nonergodic glassy state at lower temperatures by two crystal nucleation regimes; heterogeneous nucleation at higher temperatures and homogeneous nucleation at lower temperatures. In PEO_{114}-*b*-PCL_{88} both nucleation processes are soleley ascribed to PCL, which is the only crystallizable component under conditions of double confinement. The liquid-to-glass temperature also refers to the freezing of the local segmental dynamics of the more polar PCL block. Interestingly, there seems to be a minimum in the $T_g(1/d)$ dependence at round 50 nm pores. In addition, homogeneous nucleation occurs in the vicinity of the liquid-

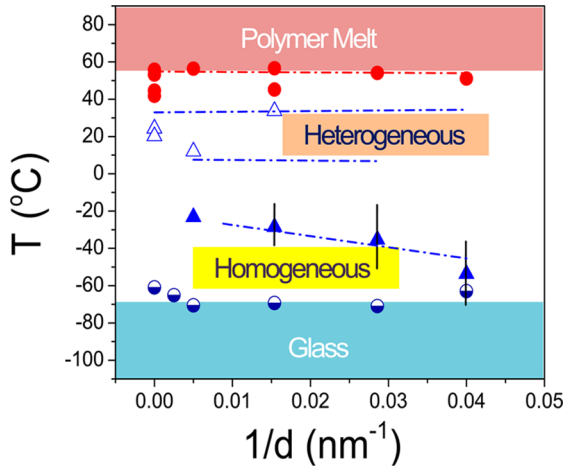

Figure 10. "Phase diagram" of PEO_{114}-*b*-PCL_{88} within self-ordered AAO based on DSC measurements and dielectric spectroscopy (liquid-to-glass temperatures). Filled spheres denote apparent melting temperatures obtained by DSC. Open and filled triangles denote temperatures at which crystallization of PCL is initiated by heterogeneous and homogeneous nucleation, respectively. Liquid-to-glass temperatures (half-filled spheres) obtained by DS are operationally defined as corresponding to 100 s. Horizontal dashed lines give the range of heterogeneous nucleation for bulk PCL. The dashed line in the vicinity of homogeneous nucleation is a guide for the eye.

to-glass temperature. For PEO_{114}-*b*-PCL_{88} inside 25 nm pores, PCL homogeneous nucleation is located only 10 K above the corresponding T_g. This finding is a further confirmation of the close relation between the spatiotemporal fluctuations associated with the liquid-to-glass temperature and the onset of homogeneous nucleation. In this picture, homogeneous nucleation is controlled by the faster segments in the distribution of relaxation times associated with the α-process.

IV. CONCLUSIONS

PEO and PCL are well-known semicrystalline polymers that show bulk crystallization initiated by heterogeneous nucleation. However, in very asymmetric PCL-*b*-PEO block copolymers, the minority block PEO nucleates at much lower temperatures via homogeneous nucleation. When the same diblock copolymers reside inside nanoporous AAO, the nucleation of the minority block PEO is completely suppressed. In this case, PEO experiences a double confinement by PCL crystals already formed at higher temperatures and by the rigid AAO pore walls. The majority block (PCL) is also affected by confinement and crystallizes at lower temperatures via homogeneous nucleation. Similar to the case of PCL homopolymer crystallized inside AAO, the PCL blocks of PEO-*b*-PCL have their {110} and {200} faces preferentially oriented normal to the AAO pore axes.[6] In addition, the confinement imposed by the rigid AAO pore walls on PEO-*b*-PCL affects molecular dynamics in that PCL segmental dynamics is accelerated and the distribution of relaxation times associated with the PCL segmental process is broadened.

These findings can be discussed with respect to the pertinent (T vs $1/d$) "phase diagram". In the proposed diagram the equilibrium melt state is separated by the low temperature nonergodic (glassy) state by two intermediate metastable states associated with different nucleation regimes; heterogeneous nucleation in the vicinity of the equilibrium melt state and homogeneous in proximity to the glassy state. This picture

dx.doi.org/10.1021/ma4026477 | *Macromolecules* 2014, 47, 1793−1800

suggests a close relation between the spatiotemporal heterogeneities associated with the liquid-to-glass temperature and the homogeneous nucleation regime. We propose that it is the fast part of the distribution of PCL segmental relaxation times that is associated with the process of homogeneous nucleation.

■ ASSOCIATED CONTENT

Supporting Information

WAXS patterns of PEO-*b*-PCL and DS spectra of PEO-*b*-PCL and representative fits. This material is available free of charge via the Internet at http://pubs.acs.org.

■ AUTHOR INFORMATION

Corresponding Author

*E-mail: gfloudas@cc.uoi.gr.

Notes

The authors declare no competing financial interest.

■ ACKNOWLEDGMENTS

The current work was supported by the Research unit on Dynamics and Thermodynamics of the UoI cofinanced by the European Union and the Greek state under NSRF 2007-2013 (Region of Epirus, call 18) and the operational program of the NSRF "Aristeia". M.S. gratefully acknowledges financial support from the German Research Foundation (STE 1127/13 and INST 190/134-1). H.D. gratefully acknowledges Max-Planck-Gesellschaft (MPG) for the financial support of the MPIP-TOBB ETU Partner Group Program. Sample preparation by C. Hess and H. Tobergte as well as SEM investigations by G. Glasser are gratefully acknowledged.

■ REFERENCES

(1) Binder, K.; Horbach, J.; Vink, R.; de Virgiliis, A. *Soft Matter* **2008**, *4*, 1555.
(2) Alcoutlabi, M.; McKenna, C. B. *J. Phys.:Condens. Matter* **2005**, *17*, R461.
(3) Howard, M. P.; Milner, S. A. *Macromolecules* **2013**, *46*, 6593.
(4) Duran, H.; Steinhart, M.; Butt, H.-J.; Floudas, G. *Nano Lett.* **2011**, *11*, 1671.
(5) Suzuki, Y.; Duran, H.; Steinhart, M.; Butt, H.-J.; Floudas, G. *Soft Matter* **2013**, *9*, 2621.
(6) Suzuki, Y.; Duran, H.; Akram, W.; Steinhart, M.; Floudas, G.; Butt, H.-J. *Soft Matter* **2013**, *9*, 9189.
(7) Massa, M. V.; Dalnoki-Veress, K. *Phys. Rev. Lett.* **2004**, *92*, 255509−1.
(8) Loo, Y.-L.; Register, R. A.; Ryan, A. J. *Phys. Rev. Lett.* **2000**, *84*, 4120.
(9) Reiter, G.; Castelein, G.; Sommer, J.-U.; Röttele, A.; Thurn-Albrecht, T. *Phys. Rev. Lett.* **2001**, *87*, 226101−1.
(10) Woo, E.; Huh, J.; Jeong, Y. G.; Shin, K. *Phys. Rev. Lett.* **2007**, *98*, 136103−1.
(11) Röttele, A.; Thum-Albrecht, T.; Sommer, J.-U.; Reiger, G. *Macromolecules* **2003**, *36*, 1257−1260.
(12) Sun, Y.-S.; Chung, T.-M.; Li, Y.-J.; Ho, R.-M.; Ko, B.-T.; Jeng, U.-S.; Lotz, B. *Macromolecules* **2006**, *39*, 5782.
(13) Steinhart, M.; Senz, S.; Wehrpohn, R. B.; Gösele, U.; Wendorff, J. H. *Macromolecules* **2003**, *36*, 3646.
(14) Michell, R. M.; Lorentzo, A. T.; Müller, A. J.; Lin, M.-C.; Chen, H.-L.; Blaszczyk-Lezak, I.; Martin, J.; Mijangos, C. *Macromolecules* **2012**, *45*, 1517−1528.
(15) Michell, R. M.; Blaszczyk-Lezak, I.; Mijangos, C.; Müller, A. J. *Polymer* **2013**, *54*, 4059.
(16) Martin, J.; Nogales, A.; Mijangos, C. *Macromolecules* **2013**, *46*, 7415.
(17) Elmahdy, M. M.; Chrissopoulou, K.; Afratis, A.; Floudas, G.; Anastasiadis, S. H. *Macromolecules* **2006**, *39*, 5170.
(18) Chen, K. J.; Wang, B.; Guan, J.; Granick, S. *ACS Nano* **2013**, *7*, 8634.
(19) Deres, A.; Floudas, G. A.; Müllen, K.; Van der Auweraer, M.; De Schryver, F.; Enderlein, J.; Uji-i, H.; Hofkens, J. *Macromolecules* **2011**, *44*, 9703.
(20) Masuda, H.; Fukuda, K. *Science* **1995**, *268*, 1466.
(21) Masuda, H.; Hasegawa, F.; Ono, S. *J. Electrochem. Soc.* **1997**, *144*, L127.
(22) Masuda, H.; Yada, K.; Osaka, A. *Jpn. J. Appl. Phys.* **1998**, *37*, L1340.
(23) Steinhart, M. *Adv. Polym. Sci.* **2008**, *220*, 123.
(24) Duran, H.; Gitsas, A.; Floudas, G.; Mondeshki, M.; Steinhart, M.; Knoll, W. *Macromolecules* **2009**, *42*, 2881.
(25) Hadjichristidis, N.,; Pispas, S.; Floudas, G. *Block copolymers: synthetic strategies, physical properties and applications*: John Wiley & Sons, Inc.: New York, 2003.
(26) Müller, A. J.; Balsamo, V.; Arnal, M. L. *Adv. Polym. Sci.* **2005**, *190*, 1.
(27) Michell, R. M.; Lorenzo, A. T.; Müller, A. J.; Lin, M.-C.; Chen, H.-L.; Blaszczyk-Lezak, I.; Martin, J.; Mijangos, C. *Macromolecules* **2012**, *45*, 1517.
(28) Shi, A.-C.; Li, B. *Soft Matter* **2013**, *9*, 1398.
(29) Floudas, G.; Reiter, G.; Lambert, O.; Dumas, P. *Macromolecules* **1998**, *31*, 7279.
(30) Floudas, G.; Reiter, G.; Lambert, O.; Dumas, P.; Yeh, F.-J.; Chu, B. Scattering from Polymers. *ACS Symp. Ser.* **2000**, *739*, 448.
(31) Jiang, S.; He, Ch.; Men, V.; Chen, X.; An, L.; Funari, S. S.; Chan, C.-M. *Eur. Phys. J. E.* **2008**, *27*, 357.
(32) Grigoriadis, C.; Duran, H.; Steinhart, M.; Kappl, M.; Butt, H.-J.; Floudas, G. *ACS Nano* **2011**, *11*, 9208.
(33) Duran, H.; Hartmann-Azanza, B.; Steinhart, M.; Gehrig, D.; Laquai, F.; Feng, X.; Müllen, K.; Butt, H.-J.; Floudas, G. *ACS Nano* **2012**, *6*, 9359.
(34) Kremer, F.; Schönhals, A. *Broadband Dielectric Spectroscopy*; Springer: Berlin, 2002.
(35) Floudas, G.; Paluch, M.; Grzybowski, A.; Ngai, K. L. Molecular Dynamics of Glass-Forming Systems. *Effects of Pressure*; Springer: Berlin, 2011.
(36) Floudas, G. Dielectric Spectroscopy In *Polymer Science: A Comprehensive Reference*; Matyjaszewski, K., Möller, M. Eds.; Elsevier BV: Amsterdam, 2012; Vol. 2.32, pp825−845,
(37) Duran, H.; Gitsas, A.; Floudas, G.; Mondeshki, M.; Steinhart, M.; Knoll, W. *Macromolecules* **2009**, *42*, 2881.
(38) Havriliak, S.; Negami, S. *Polymer* **1967**, *8*, 161.
(39) Takahashi, Y.; Sumita, I.; Tadokoro, H. *J. Polym. Sci. Polym. Phys. Ed.* **1973**, *11*, 2113.
(40) Bittiger, H.; Marchessault, R. H.; Niegisch, W. D. *Acta Crystallogr.* **1970**, *B26*, 1923.
(41) Baysal, B. M.; Stockmayer, W. H. *Macromolecules* **1994**, *27*, 7429. Jones, A. A.; Brehm, G. A.; Stockmayer, W. H. *J. Polym. Sci.* **1974**, Symp. No *46*, 149.
(42) Yamaguchi, N.; Sato, M. *Polym. J.* **2009**, *41*, 588.
(43) Gedde, U. W. *Polymer Physics*: Chapman & Hall: London and New York, 1995.
(44) Strobl, G. *Rev. Mod. Phys.* **2009**, *81*, 1287.
(45) Mark, J. E. *Physical Properties of Polymers Handbook*, 2nd ed.; Springer: Berlin, 2007; p 636.
(46) Hamley, I. W. *J. Phys.: Condens. Matter* **2001**, *13*, R643−R671.
(47) Thomas, E. L.; Anderson, D. M.; Henkee, C. S. *Nature* **1988**, *334*, 598.
(48) Petychakis, L.; Floudas, G.; Fleischer, G. *Europhys. Lett.* **1997**, *40*, 685.